



Effect of friction stir welding (FSW) parameters on the peak temperature and the residual stresses of aluminum alloy 6061-T6: numerical modelisation

Mustapha Kaid¹ · Mokhtar Zemri¹ · Abdessamad Brahami¹ · Samir Zahaf²

Received: 19 October 2018 / Accepted: 8 January 2019 / Published online: 12 January 2019
© Springer-Verlag France SAS, part of Springer Nature 2019

Abstract

In this paper, numerical modelisation of thermo mechanical behavior of FSW process of 6061-T6 aluminum alloy were performed. A three dimensional (3D), transient, non-linear structural-thermal model was developed using ANSYS software to simulate the distribution of the temperature and the mechanical stresses during FSW of the aluminum alloy. The simulated temperature distributions (profile and peak temperature) and the residual stress were compared with experimental values. The results of the simulation are in good concurrence with that of experimental results.

Keywords FSW process · Numerical modelisation · Residual stress · Temperature · Welding parameter

1 Introduction

Friction stir welding (FSW) is a solid-state joining technology patented by The Welding Institute (TWI) in 1991 [1], which is recognized as a better process for joining similar and dissimilar metals and alloys with different physical, chemical, and mechanical properties [2]. The process is illustrated in Fig. 1, where a rotating cylindrical shouldered tool plunges into the butted plates and locally plasticizes the joint region during its movement along the joint line that causes a join between the work pieces. In this process, the heat is originally derived from the friction between the welding tool (including the shoulder and the pin) and the welded material, which causes the welded material to soften at a temperature less than its melting point. The softened material underneath the

shoulder is further subjected to extrusion by the tool rotational and transverse movements.

At present, the FSW technique is a novel green manufacturing technique due to its energy efficiency and environmental friendliness, and it is widely used due to its many advantages over other welding technologies. These advantages include eco-friendliness (no use of shielding gas, no spatter produced during the process, no fumes generated), use of non-consumable tools, elimination of filler material, elimination of shielding gas, and minimal human intervention [3]. Efforts are underway made to study how FSW can be used to manufacture aircraft, ship and automobile body parts [4]. To date, many effort has been made to study the manufacturing issues encountered in the implementation of the FSW technique for industries. This implementation may lead to an interaction between many factors. As described by Mohammad [5], the interactions in his model can be expressed by relationships between the machine, tool holder, material and limitations, that is graphically summarized in Fig. 2. This model complements and extends other works by including the effect of different machines and type of tool holders. For this reason, proposing a numerical model to predict the behavior of FSW process has become paramount, in order to correlate the interaction of some of these parameters.

Finite element modelling (FEM) of the FSW process leads to a better understanding of the effect of the process parameters on the welding process and the weld seam properties. Nowadays, FSW finite element models can be classified into

✉ Abdessamad Brahami
abdouda2002@gmail.com

Mustapha Kaid
mustapha_kaid@yahoo.fr

Mokhtar Zemri
mzemri@gmail.com

Samir Zahaf
zahafsamir1983@gmail.com

¹ Laboratoire de Matériau et des Systèmes Réactifs, Université de Djillali Liabes, Sidi Bel Abbès, Algeria

² Department of Mechanical Engineering, University of Sciences and Technology, Oran, Algeria

Fig. 1 A schematic illustration of FSW process

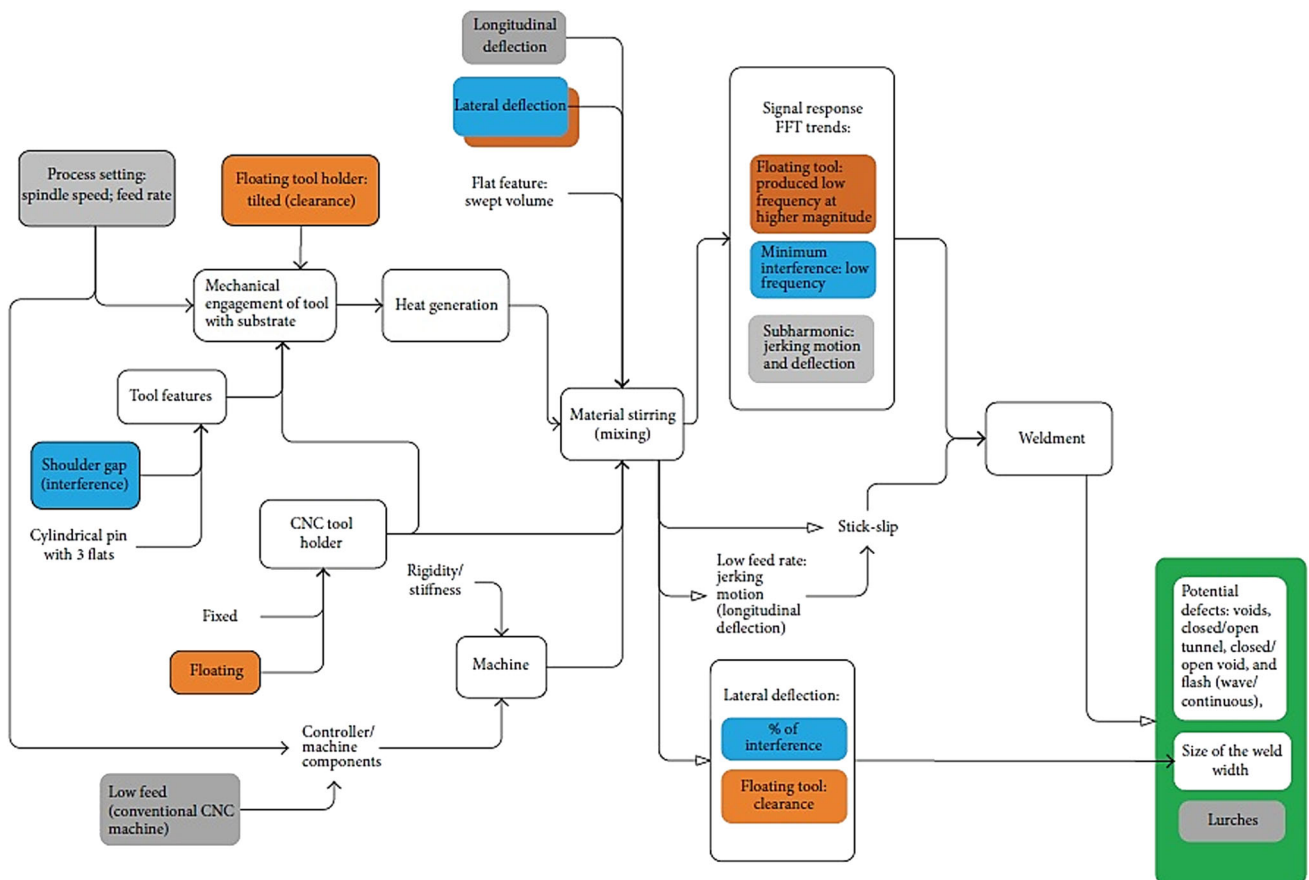
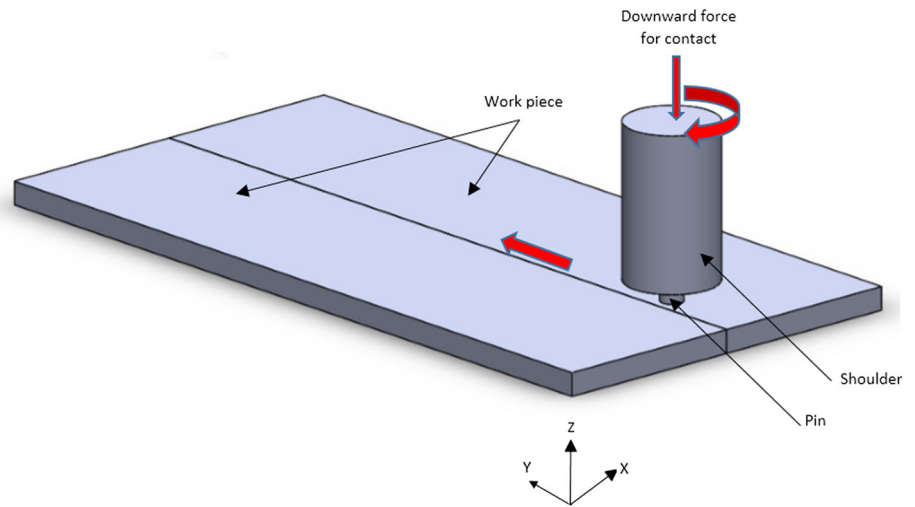


Fig. 2 A causal model for bobbin friction stir welding on selected factors

three types: thermal, thermo-mechanical non-flow base, and thermo-mechanical flow-based models [6]. In flow-based models, traditional Lagrangian elements become highly distorted and results may lose accuracy. In order to avoid high mesh distortion, several modelling techniques are often used: adaptive re-meshing and Arbitrary Lagrangian–Eulerian

(ALE). Flow-based models are developed using computational fluid dynamics (CFD). Among the main drawbacks in CFD simulations is its inability to include material hardening as it only considered rigid-viscoplastic material behaviour [7]. Flow-based models are also developed using Coupled Eulerian–Lagrangian method. This analysis technique com-

bines two approaches, Lagrangian and Eulerian: the tool steel is modelled as rigid isothermal Lagrangian body, while the workpiece is modelled using Eulerian formulation [6]. The interaction behaviour between the two is modelled by contact definition.

In the present work, three-dimensional nonlinear thermo-mechanical simulations for the FSW of AA6061-T6 using the finite element analysis were conducted. Based on the experimental results of [8–10] we have choose the rotational speeds of 500 rpm and tool feed rates of 140 mm/min so that we can compare and validate the F.E model. The coordinate system adopted in our case is related to the work piece. Based on the three-dimensional finite element method FEM a code is developed to predict the temperature and residual stresses. The results for both temperature and residual stresses are compared with the available experimental data to validate the present modelisation.

2 Numerical model and materials

The welding process is shown in Fig. 1, where V is the traverse speed of the tool, and w is its rotational speed. The tool is made of AISI A2 steel, and consists of the shoulder with the diameters of $R_0 = 16$ mm. The welded plates are 6061-T6 Al alloy, each is in a rectangular shape with a size of $200 \times 50 \times 3.18$ mm. The tool is considered a rigid solid, and the workpiece is considered a ductile material characterized with elasticity, plasticity, and a kinetic hardening effect.

The present model used an explicit contact algorithm between the surface of the tool and the two plates, between two increments of time, by its tangent plane in order to significantly reduce the calculation time. Thermal and mechanical behaviors are mutually dependent and coupled together during the FSW process which is the reason to choose a nonlinear direct coupled-field analysis. The convergence criterion of algorithms for calculating the mesh speed is fixed at 0.005 and the maximum number of iterations is 30. A complete re-meshing procedure is generated every 50 increments. The calculations are performed in parallel on 7 processors.

The flowchart in Fig. 3 shows the major steps of the written program to predict the welding temperature and residual stresses generated by the FSW process.

The temperature-dependent properties of the 6061 Al alloy are used up to 571 °C based on Ref. [11], and are given in the Table 1.

The chemical composition of the 6061-T6 aluminum alloy are given in the Table 2.

2.1 Heat transfer model

At the present work, thermal and thermo-mechanical analysis is adapted, which is similar to the numerical simulation of the

conventional arc welding [16, 17]. The heat transfer analysis was performed first, and the transient temperature outputs from this analysis are saved for the subsequent thermo-mechanical analysis. In the thermal analysis, the transient temperature field T is a function of time t and the spatial coordinates (x, y, z) , and is determined by the three-dimensional nonlinear heat transfer equation [18]:

$$k \left(\frac{\partial^2 T}{\partial x^2} + \frac{\partial^2 T}{\partial y^2} + \frac{\partial^2 T}{\partial z^2} \right) + Q_{int} = c\rho \frac{\partial T}{\partial t} \quad (1)$$

k coefficient of thermal conductivity, Q_{int} internal heat source rate, c mass-specific heat capacity, ρ density of materials. Heat flux to the system is put in by a moving source on the boundary of the weld line. This heat produced by the friction contact between the pin tool and the plates is concentrated locally, and propagates rapidly into remote regions of the plates by conduction according to Eq. (1) as well as convection and radiation through the boundary. It is assumed that the heat flux, $q(r)$, is linearly distributed in the radial direction of the pin tool shoulder, and has the following form [19]:

$$q(r) = \frac{12Qr}{\pi(d_0^3 - d_i^3)} \quad \text{for } \frac{d_i}{2} \leq r \leq \frac{d_0}{2} \quad (2)$$

d_0 outside diameter of the pin tool shoulder, d_i pin diameter, Q : total heat input energy. In Eq. (2), the heat generated at the pin of tool is neglected because this heat is very small, e.g. in the order 2% of the total heat as reported by Russell and Sheercliff [11]. As such, in the analysis $d_i = 0$ in (2) was used.

Two real constants are specified to model friction-induced heat generation. The fraction of frictional dissipated energy converted into heat is modeled first; which is set to 1 to convert all frictional dissipated energy into heat. The factor for the distribution of heat between contact and target surfaces is defined next; which is set to 0.95, so that 95% of the heat generated from the friction flows into the workpiece and only 5% flows into the tool.

2.2 Thermo-mechanical model

In the thermo-mechanical analysis, the incremental theory of plasticity is employed. The plastic deformation of the materials is assumed to obey the von Mises yield criterion and the associated flow rule. The relationship of the rate components between thermal stresses, $\dot{\sigma}_{ij}$ and strains, $\dot{\epsilon}_{ij}$ is described by:

$$\dot{\epsilon}_{ij} = \frac{1+\nu}{E} \dot{\sigma}_{ij} - \frac{\nu}{E} \dot{\sigma}_{kk} \delta_{ij} + \lambda s_{ij} + \left[\alpha + \frac{\partial \alpha}{\partial T} (T - T_0) \right] \dot{T} \quad (3)$$

Fig. 3 Global flow chart of thermo mechanical modeling of the FSW process

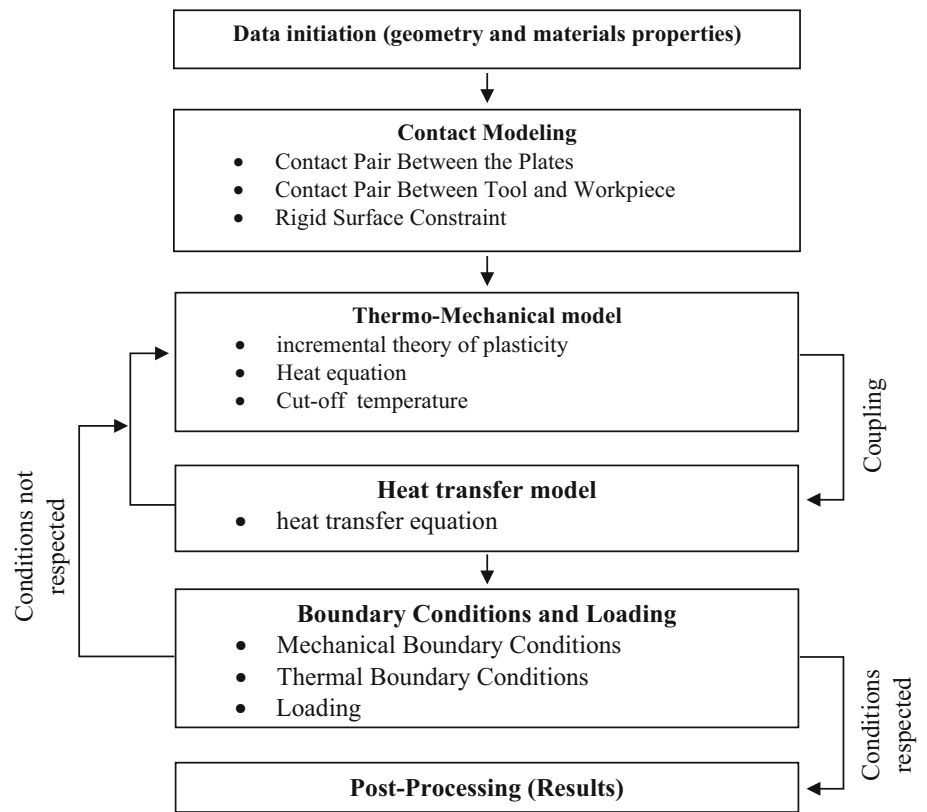


Table 1 Material properties of AISI A2 steel [12, 13] and aluminum alloy 6061-T6 [11]

	Temperature (°C)	Thermal conductivity (W/m °C)	Heat capacity (J/kg °C)	Density (kg/m ³)	Young's modulus (GPa)	Yield strength (MPa)	Thermal expansion (μm/°C)	Poisson's ratio	Melting point (°C)
AISI A2 Steel		23.8	1096	7860	203		10.6	0.23	
Al alloy 6061-T6	0	162	917	2703	69.7	277.7	22.4		
	93.3	177	978	2685	66.2	264.6	24.61		
	204.4	192	1028	2657	59.2	218.6	26.6	0.23	582–652
	315.6	207	1078	2630	47.78	66.2	27.6		
	427.7	223	1133	2602	31.72	17.9	29.6		
	571.1	253	1230	2574	0	0	34.2		

Table 2 Chemical composition AA6061-T6 [14, 15]

Mg	Si	Fe	Cu	Zn	Ti	Mn	Cr	Al
0.8–1.2	0.4–0.8	0.7	0.15–0.40	0.25	0.15	0.15	0.04–0.35	Balance

where E: Young's modulus, ν : Poisson's ratio, α : thermal expansion coefficient, $s_{ij} = \dot{\sigma}_{ij} - 1/3\dot{\sigma}_{kk}\delta_{ij}$ are the components of deviatoric stresses, λ : plastic flow factor. $\lambda = 0$ for elastic deformation or $\sigma_e < \sigma_s$, and $\lambda > 0$ for plastic deformation or $\sigma_e \geq \sigma_s$, here σ_s is the yield stress, $\sigma_e = (3/2s_{ij}s_{ij})^{1/2}$ is the von Mises effective stress.

It is well known that the thermo-mechanical analysis for welding simulation using finite element method is extremely time-consuming. To reduce computational time and still maintain reasonable accuracy, many thermo-mechanical numerical analyses use a “cut-off temperature”, i.e. the mechanical properties above the cut-off temperature are assumed to maintain constant values [17]. Tekriwal and

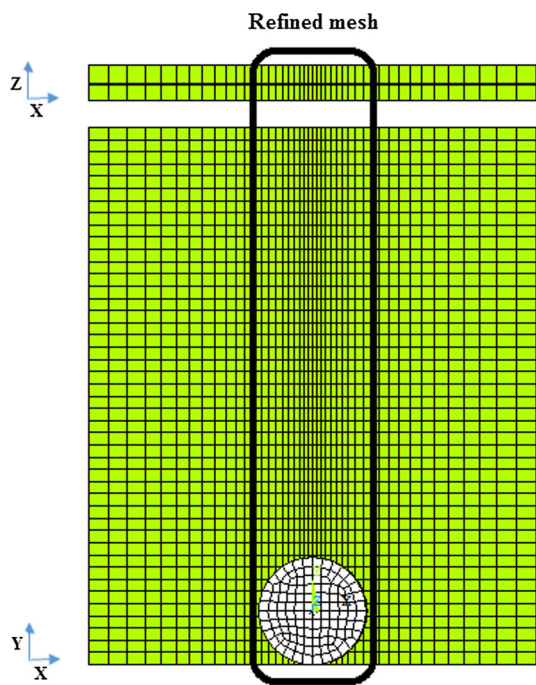


Fig. 4 Finite element model meshing

Mazumder [16] showed that the residual stresses from FEA have only small changes for carbon steels when the cut-off temperature varied from 600 to 1400 °C, but the computational time is significantly reduced if the cut-off temperature 600 °C is used. A cut-off temperature of 900 °C (i.e. about two-third of 1400 °C the melting temperature of 304L stain-

less steel) is used in the current numerical calculations to reduce unnecessary computational time.

3 Mesh, loads and boundary conditions

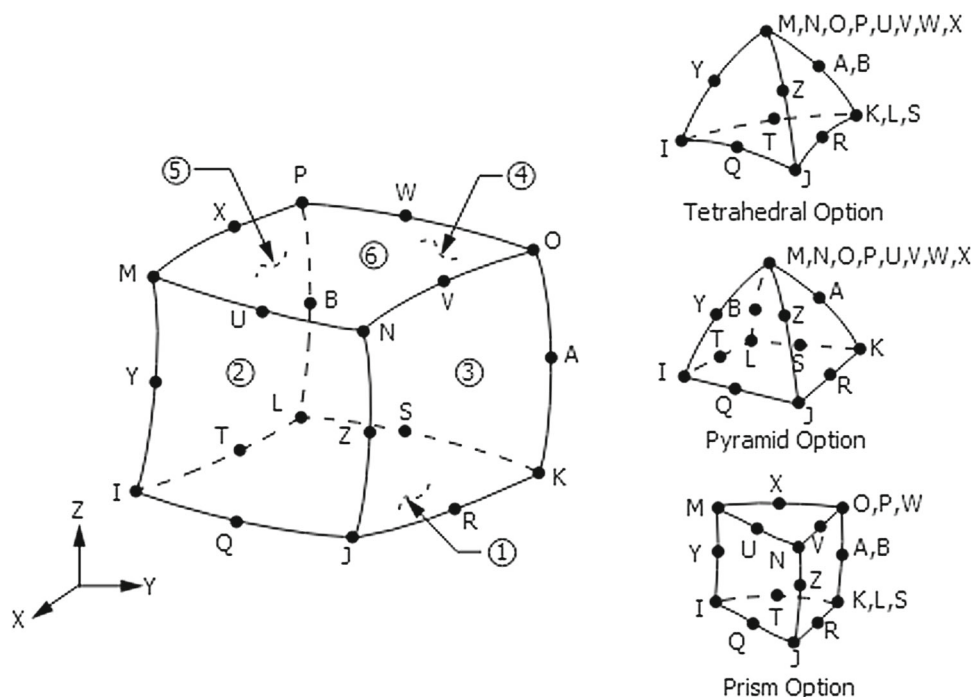
The mesh used in the calculations of the present study is a hexahedral mesh with dropped midside (quadratic interpolation functions) that can lead to oscillations in the thermal solution, leading to nonphysical temperature distribution. A hexahedral mesh is used instead of a tetrahedral mesh to avoid mesh-orientation dependency. The mesh used is composed of 7891 elements and presented in Fig. 4. The type of mesh used in this work is SOLID226, the reason for which this type of element is selected is that he has structural capabilities include elasticity, plasticity, large strain, large deflection, stress stiffening effects, pre-stress effects and structural-thermal capabilities. Figure 5 illustrate the geometry of this element.

This mesh is composed of two minimum elements in the thickness in order to take into account the gradients of the thermo-mechanical quantities according to the thickness. Near the tool, a very fine mesh zone is imposed in order to take into account the boundary layer appearing in this zone.

The boundary conditions applied to the model concern both the mechanical aspects and the thermal aspects. It is considered that we model a welding with a given speed of advance, v , and a speed of rotation of the tool, ω .

The present model, the surfaces to be joined come into contact. A standard surface-to-surface contact pair using

Fig. 5 SOLID226 geometry



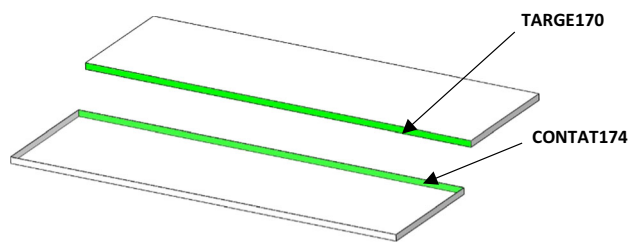


Fig. 6 The contact pair between the two surfaces

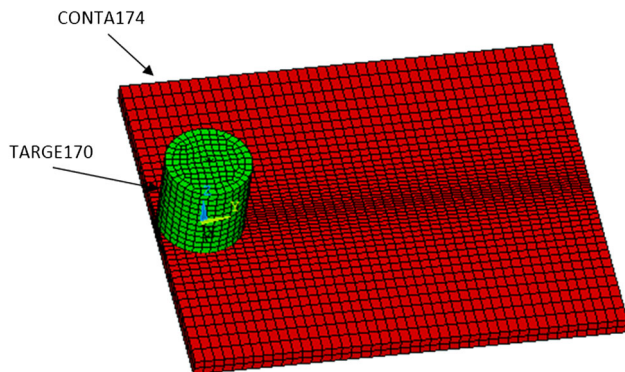


Fig. 7 The contact between the work-piece and the tool

TARGE170 and CONTA174, as shown in the following Fig. 6.

Because of the frictional contact between the tool and work-piece who is responsible for heat generation, we choose a standard surface-to-surface contact pair between the tool and work-piece. The CONTA174 element is used to model the contact surface on the top surface of the work-piece, and the TARGE170 element is used for the tool, as shown in the Fig. 7.

The thermal boundary conditions are expressed either in terms of imposed temperature or in terms of heat. They are applied on the various surfaces constituting the border:

Input: An input temperature equal to the ambient temperature, T_{amb} , is imposed.

Output: a zero heat flux, $Q = 0$, is imposed.

Lateral: a convective heat, corresponding to the exchange with the unmodeled part, is applied: $Q_{lat} = h_{lat} (T - T_{amb})$.

Lower surface: a convective heat, corresponding to the exchange with the support plate is applied: $Q_{low} = h_{low} (T - T_{amb})$.

Upper surface: a convective heat, corresponding to the exchange with air is applied: $Q_{air} = h_{air} (T - T_{amb})$ with $h_{air} = 20 \text{ W/m}^2 \text{ K}$ commonly accepted in the literature [20] (we do not take into account the clamping).

Pion and shoulder: a zero heat, $Q = 0$, is imposed.

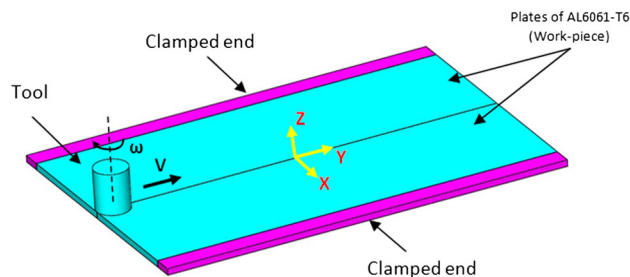


Fig. 8 Configuration and boundary conditions

The mechanical boundary conditions are expressed either in terms of imposed speed or in terms of pressure or displacement. They are applied on the various surfaces constituting the border.

we created a pilot node at the center of the top surface of the tool in order to apply the rotation and translation on the tool. The contact defined between the pilot node (TARGE170) and the nodes of the top surface of the tool (CONTA174) is defines as a Rigid Surface Constraint. A multipoint constraint (MPC) algorithm with contact surface behavior defined as bonded always is used to constrain the contact nodes to the rigid body motion defined by the pilot node.

As shown in Fig. 8, null displacements are imposed at both ends of the plates and at the bottom surface of these two plates. First, a fixed rotational speed is imposed $w = 500 \text{ rpm}$ for the tool, with a board speed equal to 2 mm/s . The feed speed of the tool is also set at 140 mm/min . The preheating time (Dwell time) is 4.5 s . These parameters are chosen to enable us to validate our numerical model with the experimental results of C Chen et al. [10].

Subsequently, we played on the welding parameters, such as angular speed and linear speed, to make a comparative study of these results. We chose angular speeds of $600, 1000, 1400 \text{ rpm}$ for a welding speed of 100 mm/s . Linear velocities of $80, 10$ and 140 mm/min for an angular velocity of $w = 1000 \text{ rpm}$ are studied.

4 Results and discussion

4.1 Heat flux

The validation of the present model was accomplished by comparing the temperature values obtained by the FE simulation with those of Chen [10]. Figure 9a shows a temperature distribution along the lateral direction (for nodes 1.5 mm below the top surface of the plate with a linear speed of 140 mm/min). It is obvious from the Fig. 9a that the numerical results found are almost identical with those of the experimental results. Figure 9b shows the cross-section temperature maps during welding.

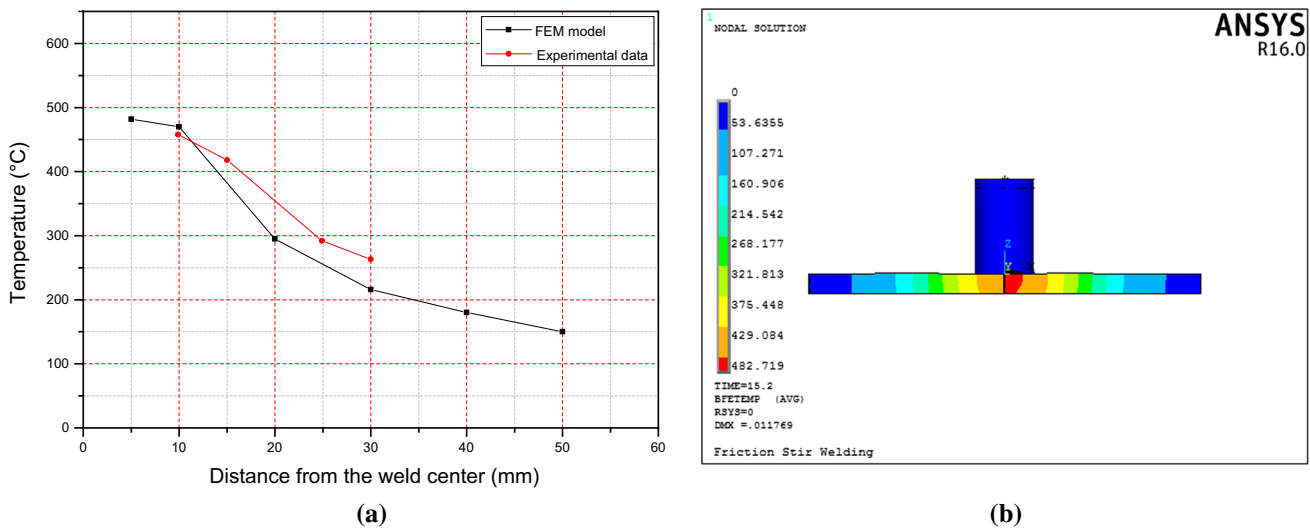


Fig. 9 Temperature evolution as a function of distance: **a** a comparison of the predicted temperature—FEM model—and the experimental data, **b** mapping of the temperature during welding

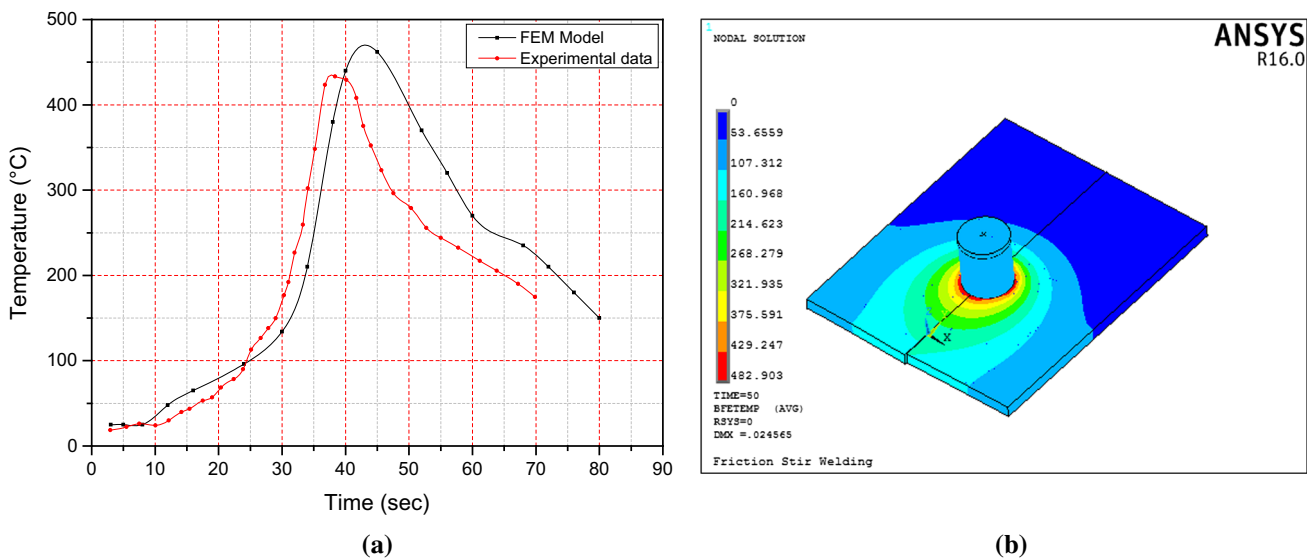


Fig. 10 Temperature evolution as a function of time: **a** a comparison of the predicted temperature—FEM model—and the experimental data, **b** mapping of the temperature during welding

We can notice that the two curves of Fig. 9a, of the numerical model and the experimental results, are very close. We note also, that the simulated maximum temperature is 482 °C, and the maximum experimental temperature is 457 °C. This shows that the maximum relative error is 6% for the maximum temperature. This value is acceptable.

Figure 10a shows a comparison of experimental data and F.E modeled value, of the temperature evolution as a function of time, for the parameter discussed above at mid position along tool movement in welding line at time 40 s. at the same time, 40 s, the temperature mapping is illustrated on Fig. 10b.

From the Figs. 10 and 11, that show a comparison between the experimental results and the F.E model, we can see that

there is a good agreement between the measured temperature and the calculated temperature, which indicates that the model developed for the prediction of the history of the temperature provides satisfactory results.

After validation of the FE model, we changed the rotation speed for a fixed linear velocity in order to see the influence of the rotation frequency on the temperature. Figure 11a shows the evolution of the temperature as a function of time for rotational speeds 1400, 1000 and 600 rpm. It is clear that each time we increase the frequency of rotation the temperature systematically increases, and this has a good agreement with the literature [21]. Figure 11b–d show the distribution

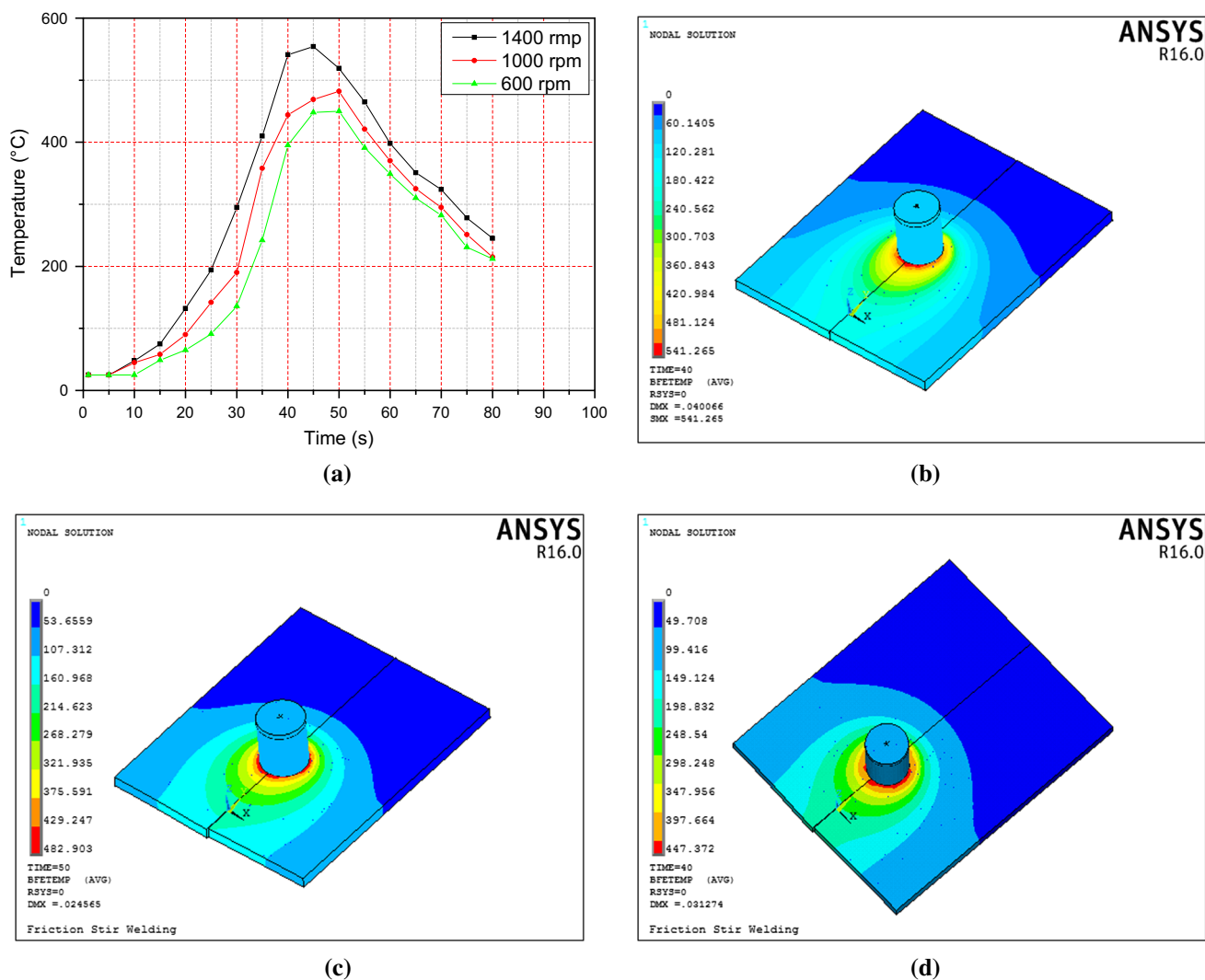


Fig. 11 Temperature evolution as a function of time: **a** a comparison of the predicted temperature of the different rotational frequency, **b** mapping of the temperature at $\omega = 1400$ rpm, **c** mapping of the temperature at $\omega = 1000$ rpm, **d** mapping of the temperature at $\omega = 600$ rpm

of the temperature at the weld at time $t = 40$ s for rotation frequencies 1400, 1000 and 600 successively.

4.2 Residual stress

The existence of the residual forces has a significant effect on the mechanical properties especially on the fatigue properties. Hence, the importance of studying the distribution of residual stresses in FSW welds. The residual stress profiles of the 80, 100 and 140 mm/min welding speeds are shown in Figs. 12, 13 and 14 respectively.

We see that for the three figures the particular profile of the component $\sigma_{res}(zz)$ is a relatively symmetrical profile containing peaks. The two extremities peaks located on either side of the zone which has been in contact with the shoulder: the maxima of the peaks are spaced apart by 20 mm

while the diameter of the shoulder is equal to 15 mm. The peak values of $\sigma_{res}(zz)$ are 122, 134 and 147 MPa for the speeds 80, 100 and 140 mm/min respectively. We made a qualitative comparison of the results found with those of the experiment of Wang et al. [22], having not considered the same welding configuration and the same aluminum alloy used by this author, we have could validate the profile with peaks, as well as the position of these peaks, located outside the area delimited by the shoulder.

Concerning the quantitative value of the residual stresses obtained, a comparison of the different welding speeds can be made, comparing the values of the residual stresses with respect to the elastic limit at ambient temperature. For the alloy in question, the elastic limit is 270 MPa, the maximum residual stresses at speeds 80, 100 and 140 mm/min are 122, 134 and 147 MPa, respectively. The estimated resid-

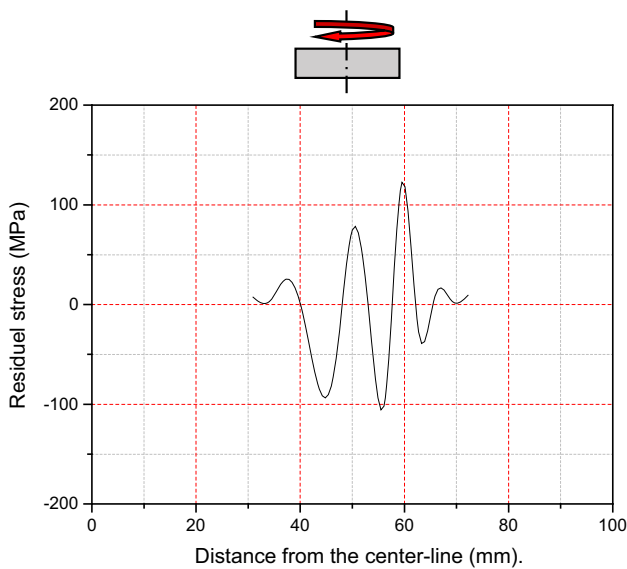


Fig. 12 Residual stress profiles as function of distance of welding speed 80 mm/min

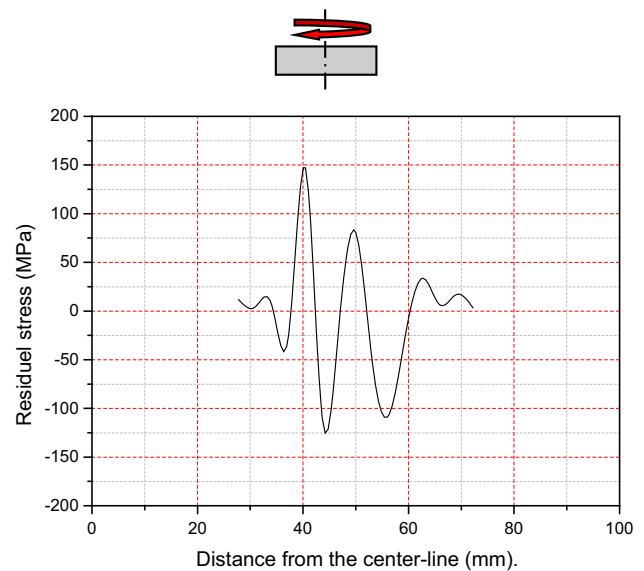


Fig. 14 Residual stress profiles as function of distance of welding speed 140 mm/min

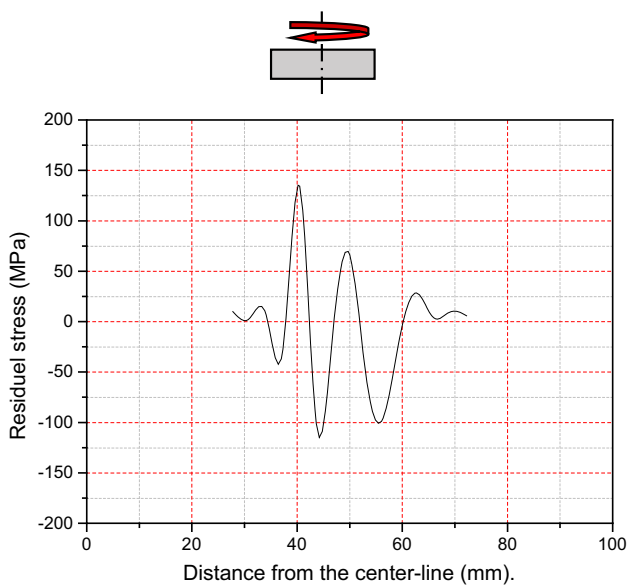


Fig. 13 Residual stress profiles as function of distance of welding speed 100 mm/min

ual stresses are thus between 45 and 54% of the yield stress at ambient temperature. In their work, Wang et al. [22] performed two tests, the first with a low welding speed, and the second with a high welding speed. They concluded that the residual stresses measured are respectively at 53% and 73% of the elastic limit taken equal to 276 MPa for a 6061-T6 aluminum alloy. Thus, the value between 45 and 54% obtained in the simulation is acceptable with regards to the experimental results. This value of 50% is also found in the works of Lawrjanie et al. [23].

4.3 Model qualification

The qualification of numerical simulation models has become increasingly important in the modeling process as the use of models has become widespread [24, 25]. Model validation consists of verifying that a model, for a given application domain, has a level of accuracy that is satisfactory and consistent with the intended application of the model. Vernat et al. [26] have developed a method of qualification of the models which implies the estimation of four parameters: Parsimony, Accuracy, precision and specialization (PEPS), that we will adopt to qualify our model. The qualification of this model by the PEPS method will make it possible to compare it to the other numerical models that simulate the FSW process.

Parsimony is a measurement which is inverse to the complexity of a model. It increases with the number and level of couplings between the variables of a model. Therefore the parsimony is the inverse of the number of relations and variables involved in the models [26].

$$Pa = \frac{1}{n_{eq} + n_{var}} \tag{4}$$

We therefore evaluate the parsimony of this model by simply taking into account the number of variables and relations of the two models; the heat transfer model and the thermo mechanical model.

The general model of interaction involves:

- 42 variables: 13 VCo et 29 VCr,
- 34 relations.

The parsimony of the model is therefore 1/76.

The literature is not rich in terms of qualification of welding simulation models, which is why we have not been able to compare the results of the parsimony of the other models.

Exactness measures the difference that separates the model from the reality it is supposed to represent. This reality refers either to the sensitive world, accessible via experiment, or to a reference behavior.

The temperature prediction of the present model is accurate up to 94% compared with experimentation. Also, residual stresses can be predicted with an accuracy up to 90%. So, in a general way, we can say that the model is really close to reality or experimentation. As a result, the model has a high exactness.

Precision is a measurement which is defined in terms of its contrast to imprecision. Imprecision measures the vague or ill-defined aspect associated with the distinction between several values for the same variable of a model, and which is represented by a group of possible values for that variable (e.g. in the form of an interval).

In the context of this study, it can be said that the imprecision of the model is due to the type and refinement of the mesh. With mesh convergence test, we can say that we obtained same results after each several tests. Hence, the model is very precise.

The Specialization of a model is represented by the hypotheses and information that restrict its area of application.

- Based on the general hypothesis of the FSW process;
- Identification of the thermal flux in the tool;
- Identification of the thermal flux in the work-piece;
- Identification of residual stresses in the work-piece;
- Identification of mechanical properties;

we can say that the model is specialized, but we cannot judge definitively on the model without comparing it with another model that simulates the FSW process.

5 Conclusion

In the present study, numerical simulation of AA6061-T6 aluminum alloys welded by FSW process under different parameter were investigated and compared with experimental data. Summarizing the main features of the results, following conclusions can be drawn:

- The peak temperature obtained from simulation is approximately near the measured one. Therefore, this heat transfer model can be used to predict the temperature distribution during the FSW process.
- The peak temperature of the welded joints increases by increasing the welding frequency rotation for the same tool profile and welding speed.
- the temperature prediction results found by the FE model, we was never reach the fusion temperature of the material in question.
- Residual stresses effected by the FSW process, moreover processing parameters responsible on the types of resultant stresses either the welding temperature and mixing.
- An increase in the welding speed apparently lead to an increase in the residual stress.
- the residual stresses found by this FE model have never exceeded the value of 54% of the elastic limit, so we can say that the model gives good results in terms of stress.

References

- Thomas, W.M., Nicholas, E.D., Needham, J.C., Murch, M.G., Templesmith, P., Dawes, C.J.: “Friction stir butt welding” International patent application no. PCT/GB92/02203 and GB patent application no. 9125978.8, 6 December 1991
- Mishra, R.S., Ma, Z.Y.: Friction stir welding and processing. *Mater. Sci. Eng. R* **50**, 1–78 (2005)
- Rodriguez, N.A., Almanza, E., Alvarez, C.J.: Study of friction stir welded A319 and A413 aluminum casting alloys. *J. Mater. Sci.* **40**, 4307–4312 (2005)
- Mahmood, H.: Ford Motor Company, 2003, www.autosteel.org accessed, 6/5/2006
- Sued, M., Pons, D.: Dynamic interaction between machine, tool, and substrate in bobbin friction stir welding. *Int. J. Manuf. Eng.* **2016**, 1–14 (2016)
- Al-Badour, F., Nesar, M., Abdelrahman, S., Bazoune, A.: Thermo-mechanical finite element model of friction stir welding of dissimilar alloys. *Int. J. Adv. Manuf. Technol.* **72**, 607 (2014)
- Al-Badour, F., Nesar, M., Abdelrahman, S., Bazoune, A.: Coupled Eulerian Lagrangian finite element modeling of friction stir welding processes. *J. Mater. Process. Technol.* **213**, 1433 (2013)
- Rodrigues, D.M., Loureiro, A., Leitao, C., Leal, R.M., Chaparro, B.M., Vilaça, P.: Influence of friction stir welding parameters on the microstructural and mechanical properties of AA 6016-T4 thin welds. *Mater. Des.* **30**(6), 1913–1921 (2009)
- Said, M.T.S.M., et al.: Experimental study on effect of welding parameters of friction stir welding (FSW) on Aluminium AA5083 T-joint. *Inf. Technol. J.* **15**(4), 99–107 (2016)
- Chen, C., Kovacevic, R.: Thermomechanical modelling and force analysis of friction stir welding by the finite element method. *Proc. Inst. Mech. Eng. Part C J. Mech. Eng. Sci.* **218**, 509–519 (2004)
- Dong, P., Lu, F., Hong, J.K., Cao, Z.: Coupled thermomechanical analysis of friction stir welding process using simplified models. *Sci. Technol. Weld. Join.* **6**(5), 281–287 (2001)
- Deng, X., Xu, S.: Solid mechanics simulation of friction stir welding process. *Trans. NAMR SME* **29**, 631–638 (2001)
- Chao, Y., Qi, X.: Thermal and thermo-mechanical modeling of friction stir welding of aluminum alloy 6001-T6. *J. Mater. Process. Manuf. Sci.* **7**(10), 215–233 (1998)
- Madhusudhan, G., et al.: Microstructure, residual stress distribution and mechanical properties of friction-stir AA 6061 aluminium alloy weldments. In: *Proc. National Seminar on Non-Destructive Evaluation*, 7–9 Dec 2006, Hyderabad

15. Brahami, A., et al.: Fatigue crack growth rate, microstructure and mechanical properties of diverse range of aluminum alloy: a comparison. *Mech. Mech. Eng.* **22**(1), 329–339 (2018)
16. Tekriwal, P., Mazumder, J.: Transient and residual thermal strain–stress analysis of GMAW. *J. Eng. Mater. Technol.* **113**, 336–343 (1991)
17. Zhu, X.K., Chao, Y.J.: Effects of temperature-dependent material properties on welding simulation. *Comput. Struct.* **80**, 967–976 (2002)
18. Radaj, D.: *Heat Effects of Welding—Temperature Field, Residual Stress, Distortion*. Springer, Berlin (1992)
19. Chao, Y.J., Qi, X.: Heat transfer and thermo-mechanical modeling of friction stir joining of AA6061-T6 plates. In: *Proceedings of the First International Symposium on Friction Stir Welding*, Thousand Oaks, CA, USA (1999)
20. Bastier, A.: *Modélisation du soudage d’alliages d’aluminium par friction et malaxage*. Ph.D. thesis, École Polytechnique, France (2006)
21. Singarapu, U., Adepu, K., Arumalle, S.: Influence of tool material and rotational speed on mechanical properties of friction stir welded AZ31B magnesium alloy. *J. Magnes. Alloys* **3**(4), 335–344 (2015)
22. Wang, X.L., Feng, Z., David, S.A., Spooner, S., Hubbard, C.R.: Neutron diffraction study of residual stresses in friction stir welds. In: *Sixth International Conference on Residual Stresses*, IOM Communications, London (2000)
23. Lawrjanie, D., Abisror, A., Decker, C., Koçak, M., Dos Santos, J.: Numerical simulation of friction stir welding. *Mater. Sci. Forum* **426**, 29932998 (2003)
24. Ordaz-Hernandez, K., Fischer, X., Bennis, F.: A mathematical representation for mechanical model assessment: numerical model qualification method. *Int. J. Comput. Math. Sci* **1**(4), 216–226 (2007)
25. Doré, R., Pailhes, J., Fischer, X., Nadeau, J.-P.: Identification of sensory variables towards the integration of user requirements into preliminary design. *Int. J. Ind. Ergon.* **37**(1), 1–11 (2007)
26. Sued, M., Pons, D.: Dynamic Interaction between machine, tool, and substrate in bobbin friction stir welding. *Int. J. Manuf. Eng.* **2016**, 1–14 (2016)

Publisher’s Note Springer Nature remains neutral with regard to jurisdictional claims in published maps and institutional affiliations.